Determination of the reference point of a radio telescope using a multilateration-based coordinate measurement prototype

Joffray Guillory, Daniel Truong, Jean-Pierre Wallerand, Michael Lösler, Cornelia Eschelbach, Swetlana Mähler, Thomas Klügel

Precision Engineering 83 (2023) 69–81

Contents lists available at ScienceDirect

Precision Engineering

journal homepage: www.elsevier.com/locate/precision

Determination of the reference point of a radio telescope using a multilateration-based coordinate measurement prototype

Joffray Guillory [a,*], Daniel Truong [a], Jean-Pierre Wallerand [a], Michael Lösler [b], Cornelia Eschelbach [b], Swetlana Mähler [c], Thomas Klügel [c]

[a] Conservatoire National des Arts et Métiers (Cnam), Laboratoire commun de métrologie LNE-Cnam, 1 rue Gaston Boissier, 75015, Paris, France
[b] Frankfurt University of Applied Sciences (FRA-UAS), Faculty 1: Architecture - Civil Engineering - Geomatics, Laboratory for Industrial Metrology, Nibelungenplatz 1, 60318, Frankfurt am Main, Germany
[c] Federal Agency for Cartography and Geodesy, Geodetic Observatory Wettzell, Sackenrieder Str. 25, 93444, Bad Kötzting, Germany

ARTICLE INFO

Handling Editor: Prof. R. Leach

ABSTRACT

A measurement campaign was carried out at the Geodetic Observatory Wettzell in order to determine the reference point of a radio telescope used for Very Long Baseline Interferometry (VLBI) at better than 1 mm. This point has been determined by measuring the trajectories of targets installed on the telescope, using two commercial total stations, but also a prototype of multilateration system composed of one absolute distance meter and of four measurement heads. The use of prototypes is always subject to risk, so the produced data must be carefully checked.

This paper evaluates independently the data from the multilateration system to ensure that they are compatible with the intended purpose. Despite the unstable position of one of the measurement heads, position uncertainties between 46 μm and 304 μm were assessed for the targets installed on the radio telescope, depending on uncertainties of the distance measurements, target visibility, and the positions of the targets relatively to the heads. These results validate the use of the multilateration system, even if the position measurements of some survey pillars of the local site network have shown larger uncertainties, of several hundred of micrometres.

At the end, the measurements of the multilateration system have been combined with those of the total stations, a global network adjustment was performed, and the coordinates of the VLBI reference point were determined with related standard deviations of 0.06 mm, 0.04 mm, and 0.10 mm for the x, y, and z axes, respectively.

1. Introduction

This contribution presents the results of a measurement campaign performed at the Geodetic Observatory Wettzell (GOW, in Germany) in October 2021 for the characterization of the southern twin radio telescope TTW-2 used for Very Long Baseline Interferometry (VLBI). VLBI is one of the most important space geodetic techniques since it is the only one realizing the celestial reference system and giving access to the time scale based on Earth's rotation (UT1). Moreover, VLBI contributes to the determination of Earth orientation parameters and global Earth-fixed geodetic reference frames.

A global geodetic reference frame, like the International Terrestrial Reference Frame (ITRF), results from the combination of several space geodetic techniques, such as VLBI, but also Doppler Orbitography and Radio positioning Integrated by Satellite (DORIS), Satellite Laser Ranging (SLR), or Global Navigation Satellite System (GNSS). For instance, GOW is a so-called core-site within the Global Geodetic Observing System (GGOS) where these different space geodetic techniques are operated. In order to combine them and to define an accurate global frame, it is essential to know the positions of these different instruments relatively to each other. This is called the local ties, i.e. vectors describing the distances and orientations between the reference points of the different techniques. Currently, the local ties have to be measured with an accuracy of 1 mm to meet the future requirements aimed by GGOS, for instance to have an accurate and stable terrestrial frame to monitor sea level change caused by climate change [1].

* Corresponding author.
E-mail address: joffray.guillory@cnam.fr (J. Guillory).

https://doi.org/10.1016/j.precisioneng.2023.05.007
Received 7 December 2022; Received in revised form 21 April 2023; Accepted 15 May 2023
Available online 18 May 2023

Whereas the reference points of DORIS beacons and GNSS antennas can be derived directly from measured reference positions, determining the VLBI reference point is a challenging task in terms of metrology. The conventional reference point of a radio telescope used for VLBI is defined as the orthogonal projection of the elevation axis onto the azimuth axis. This point lies inside the telescope structure and can neither be materialized nor measured by means of direct measurements, and indirect approaches are required, such as the trajectory measurements of the telescope antenna.

Usually, the reference point of a radio telescope is determined using conventional terrestrial geodetic instruments [2–4] such as theodolites, electronic distance metres and total stations (distance, angle and levelling measurements), or space-geodetic techniques such as GNSS [5,6]. Two examples of previous reference point determination based on terrestrial geodetic observations are presented below.

In Ref. [2], Leinen et al. presents the determination of the centre of rotation of a 35-m parabolic antenna (Cebreros, Spain). In this experiment, two targets were installed on the structure of a radio telescope, then their positions were measured by total stations (distances and angles). The observations of these targets for 6 azimuthal positions under a fixed elevation of the antenna, then 7 elevation positions under a constant azimuth, have allowed to describe the trajectories of the targets, which are circles in the three-dimensional space. From calculation of best-fitting circles, the reference point was determined with an accuracy in the range of 1–3 mm. The authors point out that the results depend mainly on the survey effort, i.e. the number of targets and positions measured, and the performance of geodetic instruments. In Ref. [3], Li et al. determines the centre of rotation of the Shanghai Tianma 65-m radio telescope. The approach is the same as before, with the measurement of 4 targets by total stations from 4 pillars, and more observations: 11 azimuthal positions under a fixed elevation of the antenna, then 8, 10 and 9 elevation positions under fixed azimuths of, respectively, 120°, 150° and 188°. The coordinates of the reference point were determined with an accuracy of the order of 1 mm.

The aim of this investigation is the determination of the reference point of the southern twin radio telescope TTW-2, at better than 1 mm, with respect to well-defined geodetic markers at GOW. To this end, Cnam has developed a coordinate measurement system dedicated to large volume metrology, called Distrimetre. It has been characterized in a meteorologic way in Refs. [7,8]: it is traceable to the International System of units (SI) and has demonstrated position accuracies between 10 μm and 45 μm, indoors, for a volume of 5.6 m × 10.3 m × 2.6 m [9]. The purpose of this investigation is to show that this instrument can also be used outdoors, on much larger volumes with distances of several tens of meters.

This instrument is based on a multilateration technique. This consists in measuring the distances that separates four laser sources, called measurement heads, to optical reflectors, called targets. If the positions of the heads are known, the coordinates of a target will then be calculated as the intersection of spheres centered on these heads and of radius the measured distances. In our case, the positions of the heads are unknown and determined by a multilateration algorithm with self-calibration: when a sufficient number of targets is measured, a system with more equations than unknowns is obtained. It is then possible to determine simultaneously the coordinates of the four heads and of the targets. In this case, the coordinate system is defined in an arbitrary way with, for example, a head that defines the origin O, a second one that defines the x axis, and a last one that defines the xy plane.

This technique is widely used in indoor industrial applications, for the calibration of machining tools [10,11], industrial robots [11], or coordinate measuring machines (CMMs) [12,13], and more generally for estimating the six-degree-of-freedom pose (position and orientation) of end effectors and ensuring the traceability of these measurements. Multilateration can be implemented using commercial instruments, such as laser tracers [10] and laser trackers (in interferometric mode [12,13] or in absolute distance meter (ADM) mode [14]), or using the Frequency Scanning Interferometry (FSI) technique [15,16]. For large volumes with distances up to 10 m, typical uncertainty levels are on the order of a few tens of micrometres. The principle of the multilateration is also known in Geodesy. For instance, GNSS-based measurement systems use this principle. However, optical multilateration is less often applied because the effort is larger (multiple stations versus a single station) in comparison to classical polar instruments (e.g. total stations), and because outdoors, i.e. in harsh environments, optical interferometry becomes ineffective due to atmospheric disturbances. Therefore, the coordinate measurement system presented in this study is based on an ADM capable of performing such measurements.

Thus, the distances are determined by an ADM based on the phase shift measurement of an intensity-modulated light at a wavelength of 1550 nm. This single ADM is connected through a 1 × 4 optical switch and a network of fibres to the four measurement heads, which act as aiming systems. These heads can therefore be several tens of meters apart from each other while measuring the same target, one after another, as shown in Fig. 1. From these heads, optical beams are propagated through the air up to the target, a hollow corner cube, then reflected on it to return to the heads and to be re-injected in the same fibres as those used for emission. The ADM can thus receive the modulated lights and determine the distances d from their phase shift ϕ as follows:

$$d = \frac{1}{2} \times \left(\frac{\phi}{2\pi} + k \right) \times \frac{c}{n \times f_{RF}} \tag{1}$$

where c the speed of light in vacuum, n the air group refractive index through which the optical beam is propagated, f_{RF} is the radio-frequency (RF) carrier of the intensity-modulated light, 5 GHz in our case, and k an integer number corresponding to the number of synthetic wavelengths $\Lambda = c/(n \times f_{RF})$ within the distance to be measured. In practice, this number is determined by a set of measurements at different RF carriers.

The reference point of the radio telescope TTW-2, depicted in Fig. 2, has been determined measuring optical retroreflectors mounted on the rotatable antenna for various azimuth and elevation positions. Basically, the trajectory of these targets allows to model the two rotation axes of the telescope, i.e. their geometry in three-dimensional space, their non-orthogonality and their eccentricity. In this way, the reference point can be determined by an orthogonal projection of the secondary axis onto the primary axis [17].

During this measurement campaign, the distances measured by the multilateration system were completed by polar measurements from commercial total stations in order to increase the number of observations and to cover a larger area of the local site network at GOW. More importantly, these additional measurements take into account other space geodetic techniques and their reference point. However, before combining all these data together, it was necessary to validate the measurements made by the multilateration system. To this end, this paper first deals with the data obtained by the multilateration system independently.

Thus, in section 2, the positioning of the measurement heads and of the different targets is presented, then in section 3, all the distance measurements performed during the 9 days of the campaign are detailed, with the corrections that have been made and the estimated uncertainties. An initial analysis based solely on the distance measurements of the multilateration system is then carried out in section 4 in order to verify the stability of the positions of the measurement heads. Indeed, the latter must be stable over time to obtain accurate target positions after data processing. In section 5, a first determination of the positions of the measured targets is performed by applying a multilateration algorithm with self-calibration that convert distance measurements into three-dimensional target coordinates. The obtained positions and uncertainties are then analysed to validate the measured distances, i.e. if they are compatible with the objective of defining the reference point of the telescope at better than 1 mm.

After this first step, in section 6, the distance measurements made by

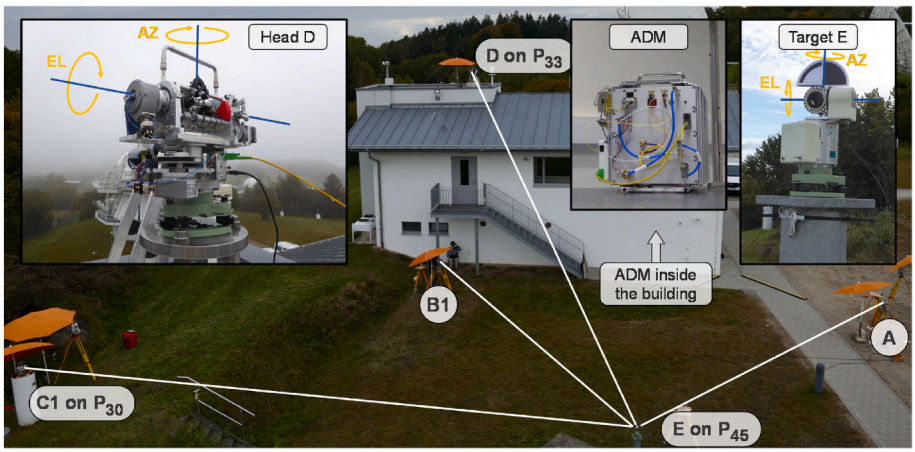

Fig. 1. Photograph of the four measurement heads, named from A to D, aiming the target E set up on pillar 45. On the top left, zoom on the measurement head D, in the middle, the absolute distance meter, and on the top right, the target E. All these devices were developed in-house.

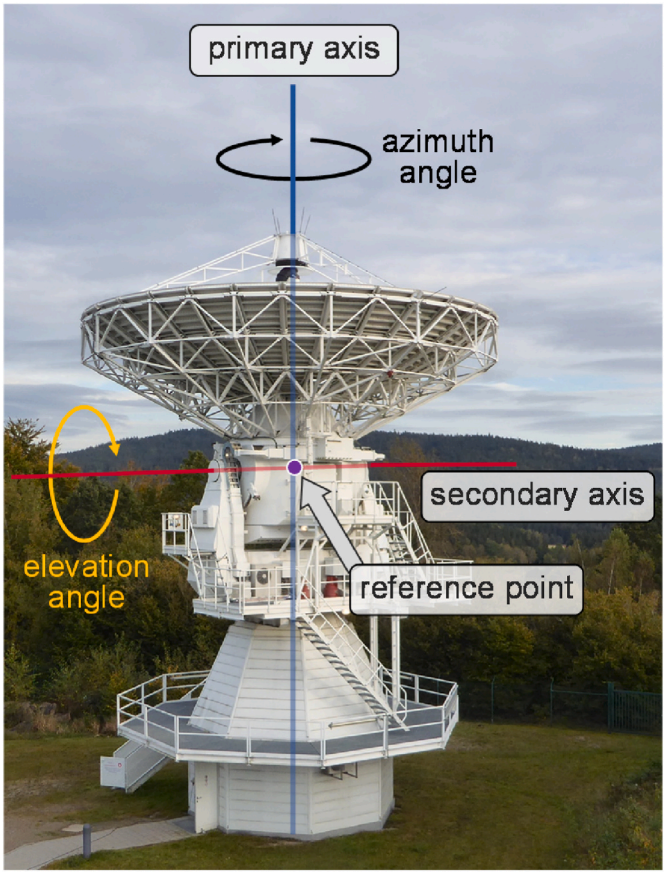

Fig. 2. Photograph of the radio telescope TTW-2 of 13.2 m diameter with its two rotating axes for azimuth and elevation angles at 90°. The secondary axis is located approximately 11.5 m from the ground.

the multilateration system are finally combined with polar measurements of two total stations and processed in a new model developed by FRA-UAS to determine the reference point of the radio telescope TTW-2 in the local site network of GOW.

2. Layout of the multilateration system

The positioning of the measurement heads of the multilateration system was a challenge because it was necessary both to cover a wide range of angular positions of the radio telescope and to ensure that all the heads can observe simultaneously a maximum of targets. Moreover, we should always try to be close to one of the optimal arrangements presented in Ref. [18] to minimize the position uncertainties. In practice, the measurement heads A, B and C were positioned at ground level, whereas the head D was placed high up on the roof of a building. Thus, all the heads were not placed in a same plane, which would have penalized the multilateration algorithm.

As shown in Fig. 3, the locations of the measurement heads A and D are remained the same during the 9 days of the measurement campaign. The heads B and C, initially located to the northwest side of the radio telescope, were moved to the northeast side at the end of day 7 to improve the angular coverage of the telescope. We have therefore two sets of positions for the measurement heads: A, B1, C1 and D, then A, B2, C2 and D.

The heads C1, D, B2 and C2 have been set up on the concrete pillars numbered 30, 33, 43 and 28, respectively. The heads A and B1 have been installed on heavy tripods depicted in Fig. 4. The tripod of head B1 was mounted on 1-m-long piles positioned in the ground in order to have a high stability, even if it is located on soft soil. The tripod of head A, located on a more stable soil, was simply set 15 cm into the ground, then covered with plaster. If cracks had appeared in the plaster, this would have meant that the tripod had moved during the measurement campaign, which was not the case.

Each Leica tribrach on which the measurement heads were set up was levelled every day at the morning using a Leica GZR3 (plummet accuracy 0.5 mm at 1.5 m, i.e. 1/3 mrad). By this way, the vertical axis of the instruments was corresponding to the local plumb line. The adjustments made from one day to the next for the different pillars and the heavy tripod used by the head A were very small, which means they were stable. On the contrary, for the first five days, the level of the measurement head B1 had to be corrected. The tilt detected by the Leica GZR3 was up to three bubble increments, i.e. 1 mrad. This shows that the stability objective of the heavy tripod of head B1 has not been achieved. The movement of head B1 is probably due to the clamp holders used to attach the legs of the tripod to the piles: they were improperly mounted. Thus, the use of heavy tripods with long piles is not to be questioned, on the contrary this approach is rather adapted to soft soils, it is rather the way in which they have been mounted that has to be reconsidered. Note that the heavy tripods should ideally have been installed one week before the start of the measurement campaign.

In the multilateration system, the targets were hollow corner cubes mounted on gimbal mechanisms so that they could turn in the direction of the heads thanks to motors remotely controlled through Wi-Fi. The first target, named E and depicted in Fig. 5 on the left, is compatible with the Leica tribrachs and can therefore measure the reference survey

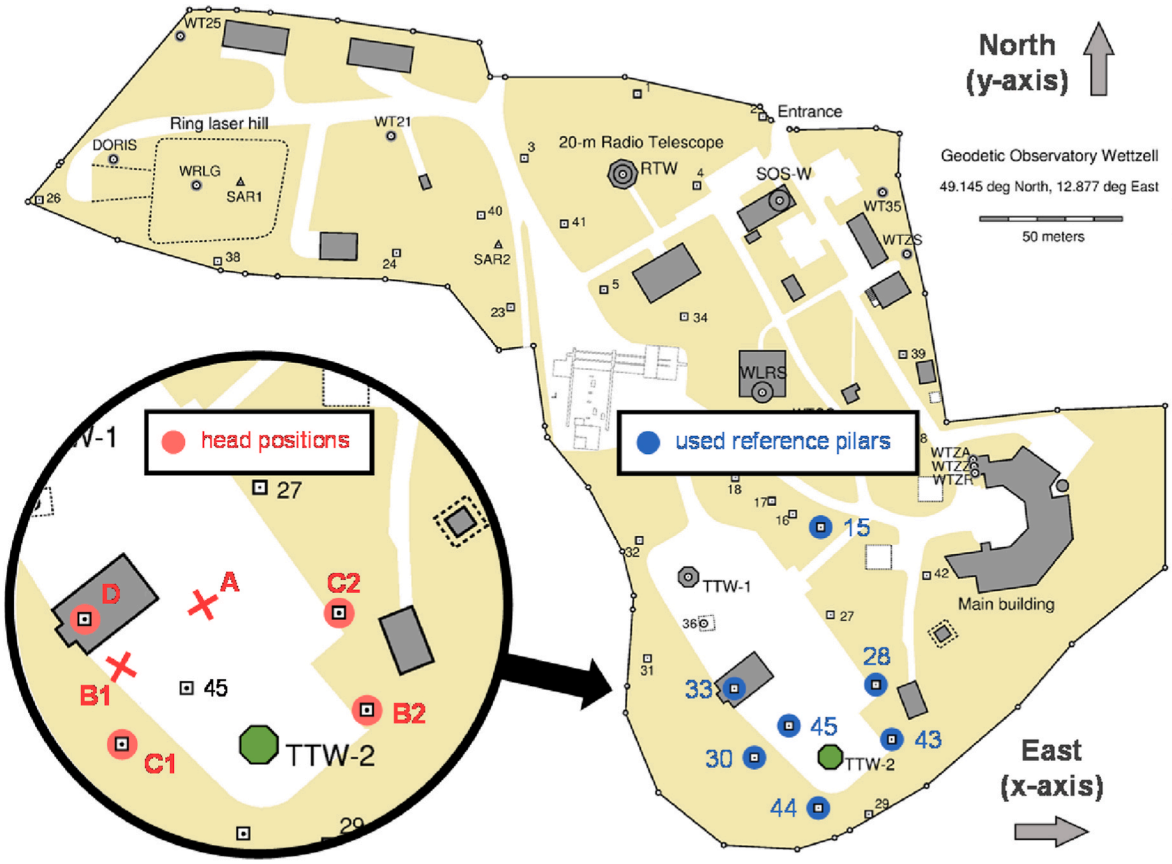

Fig. 3. Local site network at GOW with the locations of the measurement heads and pillars. The radio telescope TTW-2 is coloured in green, the pillars used in this experiment are depicted by circles (in blue for the targets and in red for the heads), and the tripods by crosses. (For interpretation of the references to colour in this figure legend, the reader is referred to the Web version of this article.)

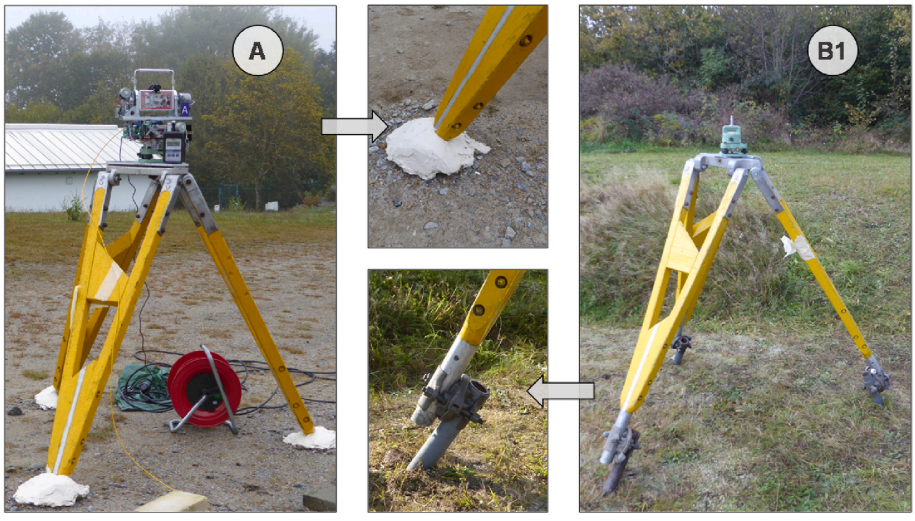

Fig. 4. Photograph of the heavy tripods used by the heads A and B1.

pillars at GOW. Then, as shown in Fig. 5 on the right, four other targets, named by letters from A to D, were used to measure their trajectories. These targets, having a different design, were attached to the structure of the radio telescope by magnetic mounts. They remained in place during all of the measurement campaign, i.e. 9 days and 8 nights, even under the rain. The target B has stopped working for a few hours on day 6, and target D has broken down during the night between the days 5 and 6. The last day, the corner cube D has been displaced to a new position which did not depend on the elevation orientation of the telescope but was still sensitive to the rotations around the telescope's azimuth axis. From then on, it is named D2 (Fig. 5, on the right). At this new location, the target D2 could be oriented manually by an operator.

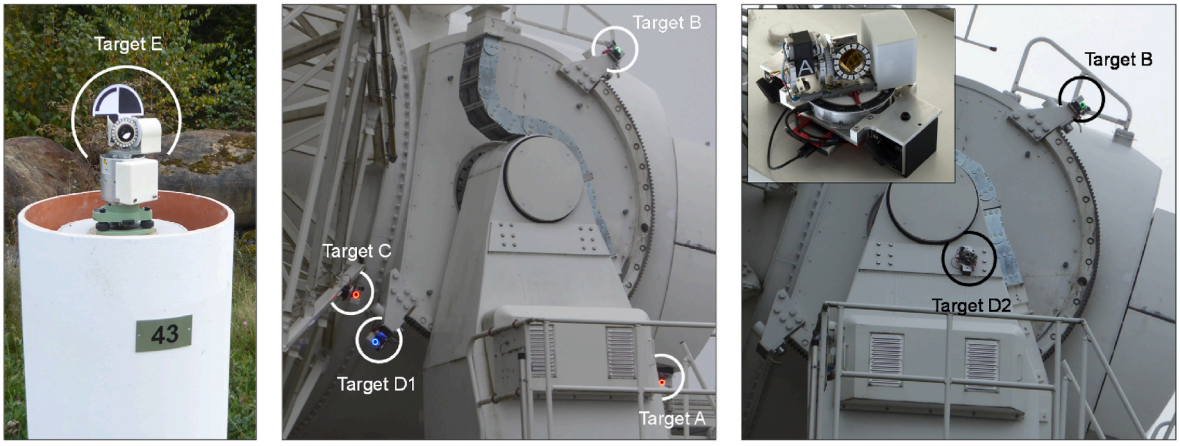

Fig. 5. Photographs of the target E mounted on the tribrachs on the left, and the ones mounted on the radio telescope (from A to D) in the middle and on the right. A zoom on the target A is also visible on the photograph of the right.

3. Data set

3.1. Distance measurements

During the 9 days of the measurement campaign at Wettzell, 101 target positions were measured with distances ranging from 12 m to 73 m. Among these positions, 69 have been measured using the four measurement heads simultaneously, 31 have been measured using only three measurement heads (trilateration), and 1 has been measured using six measurement heads simultaneously. In this last case, we took advantage of the move of the heads on day 7 to measure this target from the locations of A, B1, C1, D, then B2 and C2.

At the end, 68 different targets located on the radio telescope have been measured, 1 viewed by 6 heads, 43 viewed by 4 heads and 24 viewed by 3 heads only. The different telescope orientations that were used and the corresponding visibility of the mounted targets are summarized in Table 1.

In parallel, the target E was placed on the reference pillars 15, 28, 30, 43, 44 and 45 to determine their coordinates. This was done several times during the measurement campaign to ensure the stability of the multilateration system, by regularly checking that the distances between fixed pillars and the measurement heads were not changing from day to day. Furthermore, by using these positions and those of the heads mounted on other reference pillars, it is possible to adjust the multilateration frame to the reference frame at GOW. The coordinates of the TTW-2 reference point can thus be expressed in the right coordinate system.

Table 1
Angular positions of the radio telescope that have been measured, with the targets viewed by 3 heads in yellow, by 4 heads in green and by 6 heads in blue. In red, the target D2 measured by 4 heads, and which does not depend on the elevation axis.

Az. / El.	-85°	-60°	-30°	-15°	0°	15°	30°	60°	90°	115°	117°	152°
110°	A C					A C D	A B C	B C				
90°	A C D	A C D	A C D	A C D	A C D	A C	A B C D	A B C	C D2			B C
85°										C D2		
75°	A C							C	B C			C
65°	A					C D	B C	B C	C			B C
40°									C			
15°						C	A C	A B C			A B C D2	B
5°												B

3.2. Distance corrections

The measured distances were corrected for different sources of errors, such as the instrument offsets and the air refractive index through which the optical beams were propagated.

The instrument offsets (or zero-point offset) are lengths that are added to the measured distances to compensate for delays in electrical cables and optical paths. There is one instrument offset per measurement head, named o_i. The latter can be determined by the multilateration algorithm with self-calibration. However, in the framework of this measurement campaign, they have been measured separately thanks to a laboratory calibration. Uncertainty on these corrections were estimated to 3.6 µm.

$$\begin{cases} o_1 = 33.595 \text{ mm} \\ o_2 = 444.348 \text{ mm} \\ o_3 = 106.640 \text{ mm} \\ o_4 = 255.968 \text{ mm} \end{cases} \quad (2)$$

The second parameter to consider when assessing uncertainties is the air group refractive index through which the optical beams were propagated. It should be properly determined to deduce a geometric distance from an optical path. It is generally calculated from an update equation of the Edlén's formula [19], like Ciddor [20], which depends on the air temperature, the atmospheric pressure, the partial pressure of water vapor, and the CO_2 content. The contributions of all these parameters are presented in Table 2.

The air temperature is the parameter that contributes the most to the distance measurements as shown in Table 2. Moreover, this parameter is difficult to measure as it can vary greatly with time and position.

Table 2
Sources of errors in the air group refractive index determination based on Edlén's formula.

	Parameters	Description	Conditions	Contribution
1	ΔT	Temperature variation	Around $T = 20$ °C, $p =$ 1013.25 hPa, $RH = 50\%$ and $x_c = 450$ ppm, for $\lambda = 1550$ nm	−0.95 µm/m/°C
2	Δp	Pressure variation		0.27 µm/m/hPa
3	Δp_ω	Humidity variation		−0.09 µm/m for +10%
4	Δx_c	CO_2 content variation		0.03 µm/m for +200 ppm

Fortunately, with a generally overcast sky during the measurement campaign, the air temperature was quite stable in time and space. In fact, the sky was mainly cloudy the first days, with fog in the morning and intermittent light rains during the day. On day 4, we had a continuous light rain, with particles of water suspended in air (drizzle). In the last days, the sky was either partly cloudy or clear, so there was more sunlight.

The air temperature was measured at the level of each measurement head at the time of the distance measurements using weather stations Greisinger GFTB 100. The latter are based on platinum resistors Pt1000. The manufacturer indicates an uncertainty (type B) of 0.5% + 0.1 °C, i.e. up to 0.2 °C for the measured temperatures between 4 °C and 16 °C. These sensors have always been placed in the shade to protect them from the effects of radiation, such as solar heating outdoors. Therefore, we are confident in the temperature measurements performed at the level of the heads. However, the average temperature along an optical path may be different from that measured at the level of a head. First of all, with a generally cloudy sky during the measurement campaign, the air temperature was a priori rather stable in space. This is confirmed by the temperatures measured at the level of the heads A, B1, C1, B2, and C2, which despite different positions (their difference in altitude can be up to 2.6 m), present similar temperatures. Thus, if for each day of measurement, we adjust the temperatures measured on all these heads to a polynomial trend curve (of order 4 or 6 depending on the day), then we obtain on average residuals of standard deviation of 0.5 °C. Nevertheless, vertical temperature gradient may exist. Head D, placed high up on the roof of a building, shows temperatures with similar trends to those of the other heads, but with an average temperature higher by about 1°. In this case, the small difference of 1 °C is probably due to radiations from the heated building. Finally, we state 0.5 °C of uncertainty for the temperature measurements, which corresponds to the standard deviation of the residuals obtained between the temperature measurements in different positions and the fitting of these by a polynomial trend curve.

Besides, the relative humidities, always higher than 46%, were also measured by the Greisinger GFTB 100 sensors, the atmospheric pressures, between 944 hPa and 956 hPa, were determined by Bosch BME280 sensors, and the CO_2 contents were obtained by a Lutron GC-2028 sensor. Uncertainties of, respectively, 1.5%, 1 hPa, and 40 ppm were considered, which correspond to the manufacturer's specifications (type B).

Lastly, the distances measured from, or to, the reference survey pillars are also affected by geometric errors. Indeed, the invariant points of the gimbal mechanisms of the heads and targets do not correspond to the geodetic markers. The reference coordinates of the local site network are located vertically above the positions of the pillar screw centers, with the contact plane between the tribrach and the instrument carrier as reference height. There are therefore corrections to be made on the measured distances: corrections for the heights of the measurement heads and the target E of 188 mm, and corrections in the horizontal plane called centering errors.

To determine the centering error of a measurement head located on a survey pillar, the head with its Leica carrier has been mounted on the permanent tribrach of the pillar with all the possible angular orientations, i.e. 0°, 120° and 240°. In this way, the distances measured up to a fixed target are subject to a cyclic error. The latter does not exceed 110 µm in amplitude as depicted in Fig. 6.

The centering errors depicted in Fig. 6 have been measured with a target located in front of the pillars where the measurement heads were set up, at the same height and at a typical distance of 1 m. The measurement heads are equipped with angle encoders. Thus, the centering errors of the heads can be determined has a function of its orientation. At the end, the following centering error has to be subtracted to the measured distances:

$$correction_{CE} = a \times cos(\varphi - \pi) \times sin(\theta - \theta_0 - \theta_{CE\ 0^\circ}) \quad (3)$$

with θ and φ being the azimuth and elevation angles of the measurement heads, respectively, a and θ_0 the amplitude and the phase of the cyclic error measured in Fig. 6, and $\theta_{CE\ 0^\circ}$ the angle recorded by the azimuthal encoder during the centering error measurements when the carrier angle with the tribrach was zero (default position).

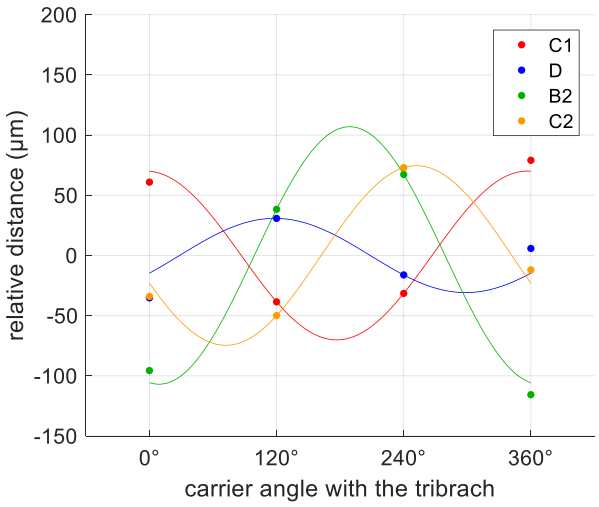

Fig. 6. Centering errors of the heads C1, D, C2 and B2 located on pillars 30, 33, 28 and 43, respectively. The dots correspond to the relative distances up to a fixed target, and the curves to the best-fitting sinusoids in the least-squares sense.

For the centering error of the target E when set up on the pillars 15, 28, 43, 44 and 45, distances to this target, using different angular orientations of this target, i.e. 0°, 120° and 240° as previously described, have been measured by the 4 measurement heads A, B1, C1 and D on day 5. Thus, the corrected positions of these reference pillars were obtained by averaging of the positions measured for each of these orientations. At the end, centering errors having amplitudes between 150 µm and 250 µm were found.

It has to be noted that such a measurement was also done with the target E set up on the pillar 30 using the measurement heads A and D. However, with only two heads, it was not possible to obtain the position corrected of the centering error.

3.3. Distance uncertainties

As demonstrated in Ref. [21], the uncertainty contribution of the telemetric system is equal to 2.1 µm (k = 1) in a controlled environment. However, the multilateration system was exposed to adverse weather conditions during this measurement campaign, with dust and rain that have increased the optical losses and the power fluctuations of the propagated optical beams. The losses directly affect the uncertainty of the telemetric system due to one of the most important parameters to take into account when assessing uncertainties: the crosstalk.

The crosstalk refers to the addition of a spurious signal to the ideal measurement signal (at the same RF frequency) due to mainly optical leakages from the emission stages to the reception ones. To evaluate the signal to crosstalk ratio (SCR), the received RF power level was recorded for each distance measurement, and the level of noise at our working frequency was measured at regular intervals. This noise depends on the measurement head, on the optical attenuation applied before reception of the signals, and it can vary randomly over time. At the end, the received RF signal was higher than −12 dBm and the SCR better than 55 dB in 75% of the cases.

From the SCR values, the uncertainty contribution of the crosstalk on the measured distances was calculated as follows:

$$u_{crosstalk} = \frac{c}{4\sqrt{2} \times \pi \times f_{RF}} \times 10^{-\frac{SCR}{20}} \quad (4)$$

Thus, with a SCR higher than 55 dB, the crosstalk adds an uncertainty contribution lower than 6.1 µm. However, in some rare cases, the SCR may be less than 40 dB and it will bring an uncertainty higher than 34.4 µm.

The other contributions of the telemetric system are presented in Table 3. They are due to a random noise, an amplitude-to-phase coupling at the level of the photodetector, or a possible shift of the RF modulation frequency locked on a rubidium atomic clock (which is limited by an aging rate of $\pm 1.5\ 10^{-9}$ per year). The uncertainties on the instrument offsets have also been taken into account and estimated to 3.6 µm, which is one of the most important contributions of the system.

As explained previously, the telemetric system measures an optical distance; and to determine the geometric distance from it, a correction for the group refractive index of the air has been made. In this case, we have considered an additional uncertainty contribution of 0.6 µm per metre mainly due to the 0.5 °C of uncertainty on the measured air temperatures.

Besides, the measurement heads and targets were not perfectly machined and assembled as with any mechanical system, which induces additional sources of error in the geometric distances. The misalignments within the gimbal mechanisms of the four measurement heads and of target E were modelled and quantified in Ref. [7] to finally show in Ref. [8] that they contribute to the uncertainty by, respectively 1.4 µm and 3.9 µm. Similar uncertainty contributions were obtained for the targets A to D.

Finally, considering additive errors for the three contributions, i.e. the telemetric system, the air refractive index, and the mechanical designs of the measurement heads and targets, the global distance uncertainties depicted in Fig. 7 are obtained. The uncertainties on the distance measurements (k = 1) are between 5.6 µm and 43.8 µm, and in 68% of the cases are lower than 20.6 µm.

Fig. 7 describes the performance of the developed multilateration system. However, there are additional sources of error that have not been taken into account. First, the uncertainties of the corrections applied to the measured distances to compensate for the centering errors of the heads have not been considered. In fact, such corrections have no impact on the uncertainty of the measured distances since they have to be considered as corrections on the survey pillar positions that will be obtained by the multilateration technique. However, this will affect the adjustment of the pillar coordinates to the local site network at GOW. Secondly, as previously explained, the measurement heads were levelled each morning, which has an impact on the positions of the heads. If the heads are considered fixed for the duration of the campaign, these levelling errors must be reported on the measured distances. This point is studied in the next part.

Table 3
Uncertainty budget of the multilateration system.

	Parameter	Description	Value	Contribution (k = 1)
1	u_{RF}	Modulation frequency	f_{RF} = 4895 MHz	$1.5 \cdot 10^{-9} \times L$
2	$u_{crosstalk}$	crosstalk	SCR from 60 dB to 40 dB	3.4 µm–34.4 µm
3	$u_{AM/PM}$	amplitude-to-phase coupling	10 dB power variations	0.4 µm
4	u_{noise}	random noise	σ_φ = 0.17 mrad	0.8 µm
5	u_{offset}	instrument offsets	formula (2)	3.6 µm
6	u_n	group refractive index of the air	Ciddor equation [20]	0.6 µm/m
7	u_{head}	mechanical design of the heads	see [7]	1.4 µm
8	u_{target}	mechanical design of the targets	see [7]	3.9 µm

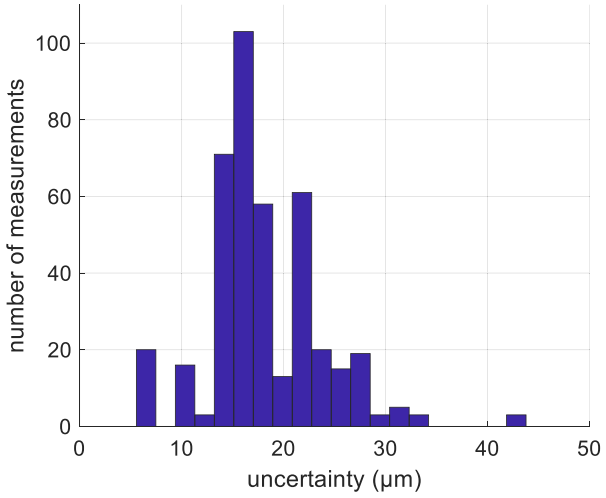

Fig. 7. Distribution of the uncertainties (k = 1) assessed for the measured distances.

4. Stability of the multilateration system

In order to check the stability of the pillars and tripods on which the heads of our multilateration system have been mounted, the distances between these heads and some reference survey pillars at GOW have been measured for several days in a row. The results for the pillars 28 and 45 are depicted in Fig. 8.

Apart from the measurement head B1, the measured distances were stable over time with variations between −130 µm and +130 µm. The related standard deviation equals to 54 µm, a value slightly larger than the distance uncertainties previously assessed in section 3.c, but which can be explained by the levelling performed each day. For the head B1, a significant drift, almost linear, is observed. The measured distances change up to 1.5 mm over 7 days for this head mounted on a heavy tripod (Fig. 4), which was clearly not stable. This is confirmed by measurements of the pillars 43 and 44 made on day 1 and day 5 as shown in Fig. 9: the maximum distance difference between these two days when observed by the heads A, C1 and D equal to 530 µm, while for head B, the difference is up to 1.3 mm for pillar 43.

These results confirm the mechanical instability of the heavy tripod on which the measurement head B was installed. Therefore, the distances measured from this head cannot be directly used.

5. Data processing

5.1. Target and measurement head positions

Since the measurement heads are equipped with angle encoders (resolution of about 400 µrad), a first approximation of the target positions can be performed in a spherical coordinate system, as for a laser tracker. Thus, in a cartesian system, the coordinates of a target j are:

$$\begin{cases} x_j = d_{i,j} \times sin(\varphi_{i,j}) \times cos(\theta_{i,j}) \\ y_j = d_{i,j} \times sin(\varphi_{i,j}) \times sin(\theta_{i,j}) \\ z_j = d_{i,j} \times \cos(\varphi_{i,j}) \end{cases} \quad (5)$$

with $d_{i,j}$ being the measured distances, $\theta_{i,j}$ and $\varphi_{i,j}$ the azimuth and elevation angles of the measurement head i when it aims at the target j.

These coordinates, accurate to a few millimetres, are used as initial values by a multilateration algorithm with self-calibration to determine the positions T_j of the targets and the positions H_i of the measurement heads using only distance measurements. This algorithm represents a nonlinear optimization problem where the quadratic sum of the differences between the squared distances measured by our ADM and the

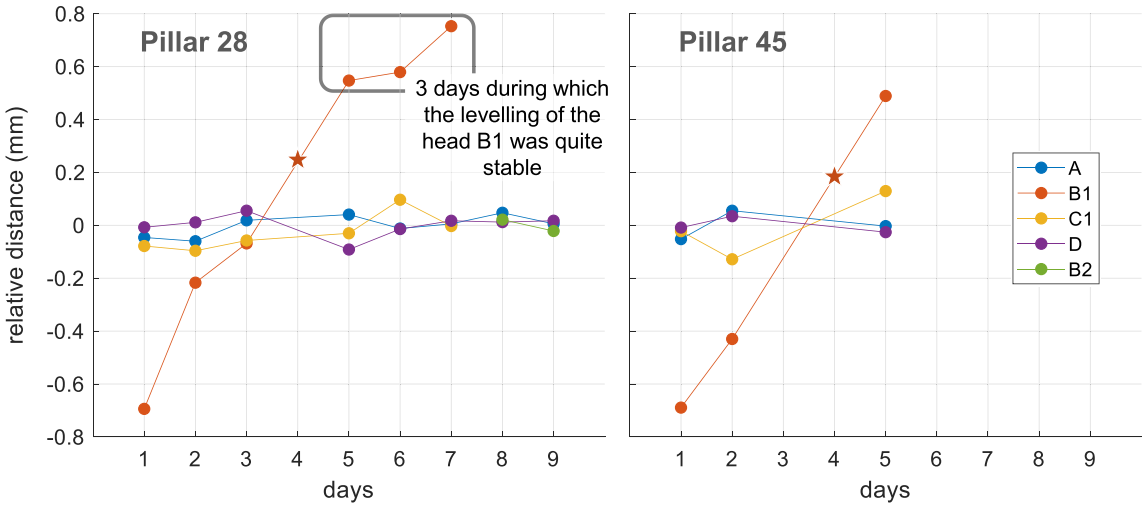

Fig. 8. Relative distances between some heads and the pillars 28 and 45. Dots correspond to measured distances, and stars to interpolated distances on day 4 for head B1.

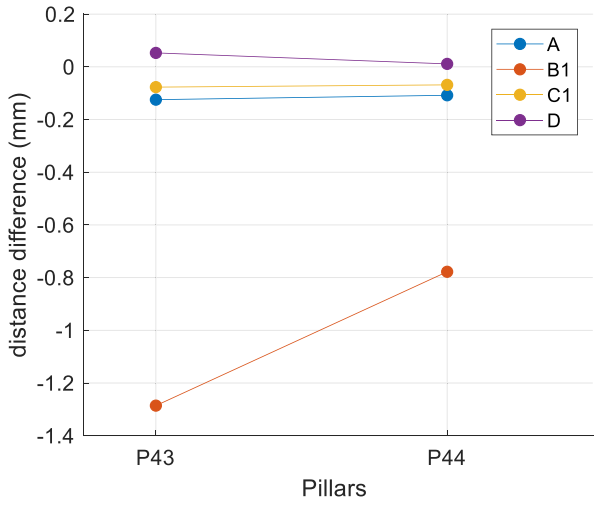

Fig. 9. Distance difference between day 1 and day 5 for pillars 43 and 44.

squared distances calculated from the positions provided by algorithm is minimized:

$$\textit{residual function} = \sum_{i,j} \left({d_{i,j}}^2 - \left\| H_i - T_j \right\|^2 \right)^2 \tag{6}$$

The unknown variables to determine are the coordinates of the 6 measurement heads and of the 70 targets measured by 4 or 6 heads. Once these are determined, the coordinates of the targets measured by only 3 heads are derived, independently, by classical trilateration.

In our case, some target positions T_j corresponding to pillars P_k, with k equals to 28, 43, 44 or 45, have been measured several times during the measurement campaign. Thus, in order to improve the multilateration algorithm, the residual function has been updated by adding the condition that the difference between two positions of a same pillar measured on different days has to be equal to zero. In the same way, distances measured with the heads A and D up to the target E set up on pillar 30 have been added as new constraints. Lastly, when a measurement head was set up on a pillar, the difference between this head and this pillar has to be equal to zero. Thus, our residual function was upgraded as follows:

$$\begin{aligned} \textit{residual function} = \sum_{i,j,k,l} \Bigg[& \frac{1}{{\sigma_{d_{i,j}}}^2} \times \left({d_{i,j}}^2 - \left\| H_i - T_j \right\|^2 \right) \\ & + \frac{1}{{\sigma_{d_{D\to 30}}}^2} \times \left({d_{H_A \to P_{30}}}^2 - \left\| P_{30,l} - H_A \right\|^2 \right) \\ & + \frac{1}{{\sigma_{d_{A\to 30}}}^2} \times \left({d_{H_D \to P_{30}}}^2 - \left\| P_{30,l} - H_D \right\|^2 \right) \\ & + \frac{1}{{\sigma_0}^2} \times \left(0^2 - \left\| P_{k,l} - P_{k,l} \right\|^2 \right) \\ & + \frac{1}{{\sigma_0}^2} \times \left(0^2 - \left\| P_{k,l} - H_i \right\|^2 \right) \Bigg]^2 \end{aligned} \tag{7}$$

with $P_{k,l}$ being the coordinates of a target T_j set up on a pillar numbered k on day l.

In order to take into account the wide variety of uncertainties that have been estimated for the measured distances (see Fig. 7), weights have been added to the residual function. The first terms of the residual function are thus divided by the square of the uncertainty on the measured distances. In addition, to ensure that two positions of the same pillar measured on different days are equal, or that a measurement head installed on a pillar has stable coordinates, we have arbitrarily opted for the last terms of the residual function for a weight much higher than the other weights with an uncertainty σ_0 of 0.25 µm, which really constrains the network.

However, this was not enough to obtain a satisfactory residual in formula (7) because, as seen previously, the measurement head B1 moved over time. To resolve this problem, a new position of the head B1 was considered each day for the 4 first days, then a new head B1 for the days 5, 6 and 7 when its tripod seemed more stable regarding the levelling carried out at the beginning of each day. Thus, as shown in the timeline in Fig. 10, ten different measurement heads are now considered.

Due to a continuous light rain on day 4, only 6 target positions were measured during that day (of which only 4 were measured by four heads). Therefore, to compensate for this lack of measurements and help the algorithm better define the position B14, the curves shown in Fig. 8 were interpolated to add two new points on day 4.

Fig. 11 presents the results after applying the multilateration algorithm with self-calibration. In this figure, the error is the difference between the distances measured by the telemetric system and the distances deduced from the multilateration algorithm that provides the coordinates of the measurement heads and targets. For each target

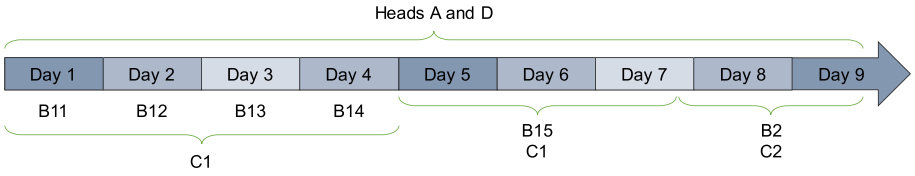

Fig. 10. Timeline of the used measurement heads.

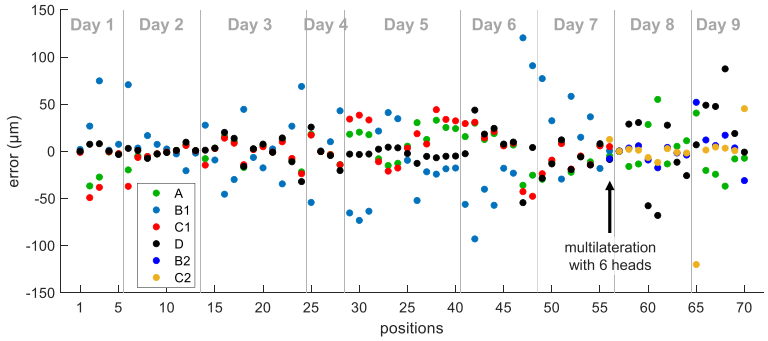

Fig. 11. Experimental results of the multilateration with self-calibration. The error is the difference between the distances measured by the telemetric system and the distances deduced from the coordinates of the measurement heads and targets provided by the multilateration algorithm. The global standard deviation on the error is 27.4 µm.

position, four errors are calculated, one per head. With errors lower than 120 µm and a standard deviation of 27.4 µm, it can be concluded that the multilateration algorithm with self-calibration converges well. Furthermore, the absolute errors are less than 20.1 µm in 68% of the cases, which is consistent with the distance uncertainties depicted in Fig. 7.

When the results are analysed in detail, the standard deviations on the errors are between 18 µm and 23 µm, except for the heads C2 and B1 which have standard deviations of 34 µm and 44 µm, respectively. Such a result is not surprising for the head B1, which was not stable. For head C2, this can be explained by the position measurement numbered 65, which appears to be incorrect. The latter corresponds to a measurement of the target E located on pillar 44, with long distances between 30 m and 46 m.

Fig. 11 shows that the measured distances are consistent with each other, and the related standard deviation of 27.4 µm is close to the uncertainties presented Fig. 7, even if it is slightly larger. The uncertainty of the temperature measurements, estimated at 0.5 °C in part 3.b, may have been underestimated. To obtain from the uncertainty budget in Table 3, 68% of the distances with an uncertainty (k = 1) less than 27.4 µm, the temperature uncertainty should be increased to 0.8 °C.

Finally, there is no unexpected error in Fig. 11 (i.e. outliers). If measurement errors had been made, the multilateration algorithm with self-calibration would not have converged as well. Therefore, it seems that the uncertainty budget was well calculated, the operator choices, such as defining a new position of head B1 for each new day, are relevant, and the weights used in the residual function are correct.

This analysis of the errors is a minimum requirement for the validation of data from such a measurement campaign, but we can go further and propagate the uncertainties of the distance measurements to three-dimensional positions.

5.2. Position uncertainties

Once the measurement head and target positions were determined, the uncertainties on these positions were assessed. The latter depend on the multilateration algorithm through which the measured distances are transformed into position values. In this process, the positions of the targets relatively to the measurement heads play an important role. The optimal configurations to minimize the uncertainties, presented in Ref. [18], are difficult to approach in practice since this partly depends on the available survey pillars. Nevertheless, it should be noted that the chosen configuration is more favourable for the targets mounted on the radio telescope than those set up on the pillars of the geodetic network.

The determination of the uncertainties on the measured positions is a complex calculation detailed in the study presented in Ref. [9]. In this paper, only the results are presented. First, the uncertainties, expressed as 3 × 3 covariance matrices, can be depicted by ellipsoids. In order to represent confidence regions of 68% probability, a scaling factor of 1.88 was applied to the eigenvalues of the covariance matrices, which allows to move from one-dimensional normal error distributions towards trivariate error distributions [22]. Fig. 12 shows two examples, one for the

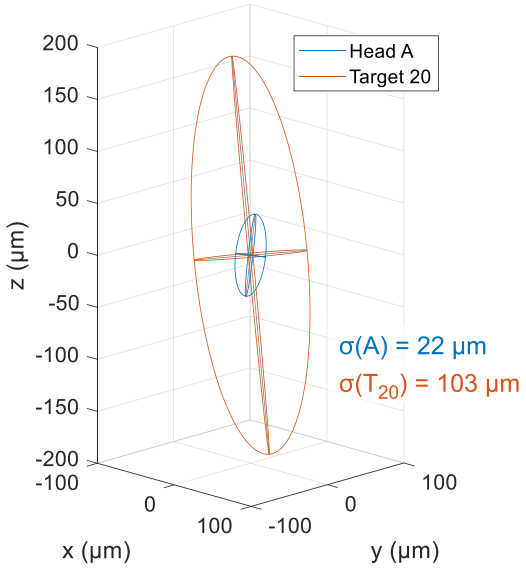

Fig. 12. Example of confidence ellipsoids describing confidence regions of 68% probability. The *x*, *y* and *z* axes are oriented as depicted in Fig. 3.

measurement head A and one for the target C measured on day 3 with the radio telescope at azimuth = −60° and elevation = +90° (position numbered 20). In the same way as these examples, the position measurements of this campaign have, in most cases, their highest uncertainty mainly oriented along the z axis (i.e. along the vertical component). This is due to small vertical variations between the heads: the maximum difference is about 9.2 m between B2 and D, but if we exclude head D we get only 2.6 m.

For a better comparison of the results, the uncertainties can also be expressed as a single number as follows:

$$\sigma_{Position}(i) = \sqrt{\sigma_x(i)^2 + \sigma_y(i)^2 + \sigma_z(i)^2} \tag{8}$$

where i is the position number. In other words, the uncertainty is the square root of the sum of the diagonal elements of the covariance matrix.

In this case, and as shown in Fig. 13, the uncertainties on the positions of the measurement heads are always lower than 130 µm, except for the measurement head B14. This corresponds to the position of head B1 on day 4, which is not well defined due to the lack of measurements during this rainy day.

Concerning the targets installed on the radio telescope, their uncertainties are less than 200 µm when they are determined by multilateration with 4 heads, and as might be expected, the uncertainties are higher when only 3 heads are used, up to 300 µm. For comparison, the target position obtained by multilateration with 6 heads, i.e. target C on day 7, has an uncertainty of 46 µm (result not depicted in Fig. 13). These levels of uncertainty, much better than 1 mm, meet the requirements for the determination of the reference point of the radio telescope TTW-2.

However, the positions of the target E set up on the survey pillars of the local site network at GOW have uncertainties of a different order of magnitude, with values between 0.27 mm and 2.32 mm. This is due to the not optimal position of these pillars relative to the measurement heads. In fact, if all the heads are located in the same place, or very close to each other, the information provided by the four measured distances will not be much greater than that provided by a single distance, and the uncertainty in the directions orthogonal to the target-head axis will be very high. In our case, the top view in Fig. 3 shows that the heads A, B1, C1 and D (multilateration before day 8) and the heads A, B2, C2 and D (multilateration after day 7) are within an angle of, respectively, 70° and 130° from the radio telescope point of view, while from the pillar point of views the heads are within smaller visual fields. Thus, the target E set up on the survey pillars has higher uncertainties, up to 2.3 mm for the pillar 15 measured by trilateration on day 5 (19° angle).

Such uncertainties can be problematic for coordinates change from the multilateration frame to the frame of the local site network at GOW. This step is, however, crucial for the determination of the local tie vectors describing the distances and orientations between the reference points of the different space geodetic techniques.

This section has highlighted a limitation of the multilateration technique: for a given configuration of the measurement heads, some target positions can be measured with an uncertainty better than 200 µm, while other target positions have an uncertainty up to 670 µm (pillar 28) or of several millimetres for trilateration (pillar 15).

5.3. Positions of measurement head B1

In order to verify whether the choice to define a new position of the head B1 for each new day was relevant, the different positions of this head obtained by the multilateration algorithm with self-calibration were plotted in Fig. 14. This head is the one set up on the heavy tripod moving over time, and it appears that this head moved upwards about 800 µm along the z axis and sidewards about 1.2 mm along the negative x axis. The results along the y axis are compatible between them with error ellipses that overlap: the observed y coordinates stay within ±100 µm. It has to be noted that the observed movement can be partly explained by the levelling of the tribrach of this head at the beginning of each day.

For sure, the movement of the heavy tripod of the head B strongly degrades the performances of the multilateration system. If a new position of the head B1 had not been considered for each new day, it would not have been possible to define the coordinates of B1 in an accurate way.

5.4. Interpoint distances

In order to validate the data from the prototype of the multilateration system, reproducibility tests were carried out. For instance, the target positions measured several times during the measurement campaign, on different days, and under different environmental conditions, or even with different measurement heads, should have the same target coordinates.

To check this reproducibility, the positions of the reference pillars 28, 43, 44 and 45, measured over several days, were first compared. For this purpose, Fig. 15 (on the left) shows for each pillar the evolution of the distances between the different measured positions and the mean position. For example, pillar 28 was measured up to day 6 using the 4 heads A, B1, C1 and D, then the last few days using only the 3 heads A, D and B2. At the end, the observed discrepancies in Fig. 15 are up to 475 µm (peak to valley), which is compatible with the assessed uncertainties in Fig. 13, between 276 µm for pillar 45 and 680 µm for pillar 28.

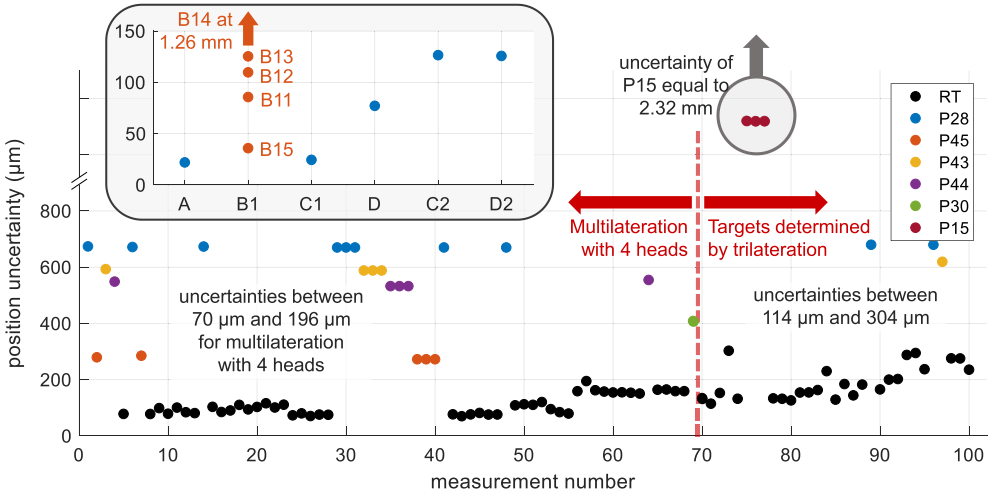

Fig. 13. Uncertainties of the measurement heads, from A to D2, and of the targets measured by 4 or 3 heads.

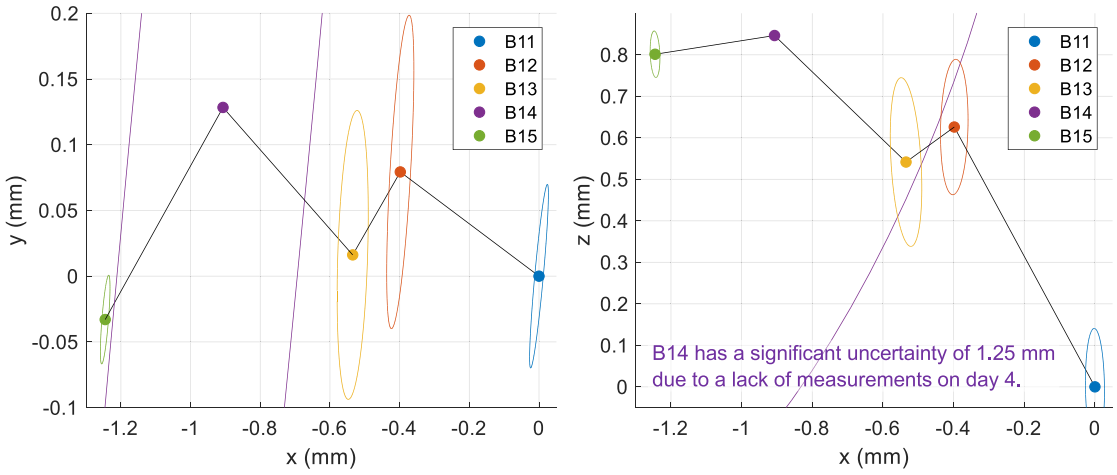

Fig. 14. Relative displacement of the measurement head B with the position of the first day as origin. The main ellipse error has been plotted to show the uncertainty level of each head.

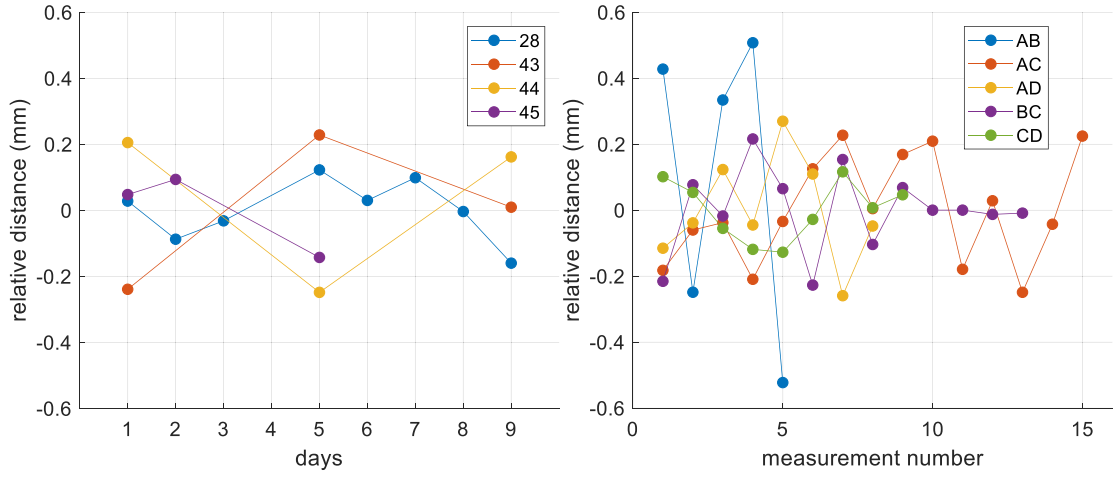

Fig. 15. Reproducibility of interpoint distances.

In a similar way, the distances measured between the different targets mounted on the radio telescope should always be the same for different orientations of the radio telescope. Fig. 15 (on the right) shows these interpoint distances. Their variations are within ±270 µm with standard deviations between 89 µm and 170 µm, except for distance AB which have a higher dispersion with variations up to 1 mm (peak to valley). No explanation was found for this larger dispersion.

Table 4 summarizes the results of distances measured between the targets mounted on the radio telescope. Only one value exists for the distance between the targets B and D, and, thus, the standard deviation is not calculable.

At the end, the reproducibility of the interpoint distances demonstrates that the data from the multilateration system are compatible with the objective of determining the reference point of the radio telescope at better than 1 mm. This also demonstrates that the positions of the targets set up on the radio telescope, and attached to the structure by magnetic systems, were stable over the 9 days of the measurement campaign.

Table 4
Distances measured between the targets mounted on the TTW-2 radio telescope and the corresponding standard deviations.

Interpoint distance	Average distance (mm)	Standard deviation (µm)
AB	2747.171	458
AC	3990.297	163
AD	2921.945	163
BC	3941.648	127
BD	3338.080	–
CD	1402.452	89

6. Determination of the reference point

The results presented in this contribution highlight the performances of the Distrimetre instrument. The uncertainties on the distances measured by the multilateration system are around 21 µm as assessed by the uncertainty budget (Fig. 7). This was confirmed by the standard deviations of the difference between the measured distances and the distances deduced from the coordinates of the measurement heads and targets provided by the multilateration algorithm (Fig. 11). However, the uncertainties are greater for the head B1 due to its mechanical instability, with an observed standard deviation of 44 µm. Besides, for the targets mounted on the radio telescope, the estimated position uncertainties and the standard deviations observed of the interpoint distances are mainly lower than 300 µm. The measurements of the multilateration system can therefore be used for the determination of the reference point of the radio telescope TTW-2. However, target positions of the survey pillars present higher uncertainties, between 270 µm and 2.3 mm.

The measurements were completed by additional measurements

performed by FRA-UAS using Leica total stations TS50 and TS60. The total stations have measured the same targets as the multilateration system, simultaneously with it. These additional measurements help to compensate for the movement of the measurement head B1 over time, up to 1.1 mm and 0.7 mm along the x and z axes, respectively, as seen previously. The polar measurements also help to improve the uncertainties on the target positions, especially those of the reference survey pillars. The data set is therefore larger than presented so far, with more than 2700 distance measurements. In this context, it makes more sense to treat all the data together in a new model developed by FRA-UAS.

For the network adjustment, all the distance measurements of the multilateration system were merged with those of the two Leica total stations TS50 and TS60, which were used for the survey of the local site network [23]. Similar strategies were used to process the data, as assigning a new position of the head B1 each new day to compensate the movement of its tripod. The sets of distances of the three instruments were introduced into the network adjustment with different weights: distance uncertainties of about 0.3 mm were set for the two total stations, and 0.1 mm for the multilateration system. These values are derived from variance component estimation [24]. For this purpose, groups of observations were formed depending on the observation type (distance or angle) and measurement instrument. Then, the variance components of these observation groups were estimated. In our case, the stochastic model was iteratively adapted until the estimated variance components were close to the expectation value $E\{\widehat{\sigma}^2\} = 1$. In the final adjustment, the variance components of the sets confirming the assumptions of the stochastic model are $\widehat{\sigma}^2_{\mathrm{TS50}} = 0.8$ and $\widehat{\sigma}^2_{\mathrm{TS60}} = 0.6$ for the two total stations, and $\widehat{\sigma}^2_{\mathrm{DM}} = 0.7$ for Distrimetre, the name given to the multilateration system. The results clearly indicate the superiority of the multilateration measurement system, which is at least three times better than a conventional total station for the telemetric unit.

The target positions extracted from this network adjustment, which combines all the measurement systems into a consistent network, were then used for the derivation of the VLBI reference point. To this end, a modified transformation approach derived by Lösler et al. [25] was applied to obtain the orthogonal projection of the elevation axis onto the azimuth axis. The conventional reference point of the radio telescope results from a transformation between a telescope-fixed reference frame and the Earth-fixed reference frame realized by the stable survey pillars of the local site network. The basic equation is:

$$\mathbf{P}_{j,k} = \mathbf{P}_{\mathrm{IRP}} + \mathbf{R}_x(\beta)\mathbf{R}_y(\alpha)\mathbf{R}^{\mathrm{T}}_z(\kappa_k)\mathbf{R}_y(\gamma)\left(\mathbf{e}_{\mathrm{AO}} + \mathbf{R}_x(\omega_k)\mathbf{p}_j\right) \tag{9}$$

where $\mathbf{p}_j$ is a certain position defined in the telescope-fixed frame and $\mathbf{P}_{j,k}$ is the corresponding position in the Earth-fixed frame observed in a specific telescope orientation given by the azimuth angle κ_k and elevation angle ω_k. α and β compensate the tilt between the azimuth axis of the telescope and the z axis of the reference frame, γ and $\mathbf{e}_{\mathrm{AO}}$ parameterize the non-orthogonality and the offset between both telescope axes, and $\mathbf{P}_{\mathrm{IRP}}$ is the position of the reference point. Matrices $\mathbf{R}$ are basic rotation matrices. For a detailed description, the reader can refer to the contributions [25,26].

At the end, the positions $\mathbf{P}_{j,k}$ cover the full azimuthal working range of 360° and almost the entire working range of the elevation angle. Treating these positions as observations, the reference point of the TTW-2 was determined by means of least-squares adjustment. The fully populated variance-covariance matrix of the positions serves as stochastic model within the adjustment. Table 5 summarizes the estimated reference position and the related standard deviations. As previously seen, a larger uncertainty is obtained along the z axis.

Table 5
Estimated reference point coordinates as well as related standard deviations.

component	value (mm)	σ (mm)
x	98 132.3	0.06
y	−156 095.8	0.04
z	15 374.3	0.10

The Global Geodetic Observing System aims for an accuracy of 1 mm for the reference points, which is reached by the described analysis procedure. In order to evaluate the benefit of the Distrimetre, the coordinates of the TTW-2 reference point were derived separately from the observed positions of the Distrimetre. This data set consists of only 10% of the full data set. The estimated reference point deviates in x, y, and z by 0.0 mm, −0.1 mm, and 0.2 mm, respectively. These small differences are insignificant compared to the derived uncertainties. In summary, reference points can be efficiently obtained from a small but precise data set, as improved instrumentation reduces both measurement effort and radio telescope downtime during the measurement campaign.

7. Conclusion

The determination of the reference points of space geodetic techniques, such as GNSS, SLR, VLBI, DORIS, is essential for the combination of these different techniques and for the realization of a global Earth-fixed geodetic reference system. The future requirements, e.g. sea level monitoring, require to know these points with an accuracy better than 1 mm.

We have developed an absolute distance meter to measure the distances that separate targets from 4 heads. This multilateration system, traceable to the SI, has been carefully optimized and characterized in a metrological way. In this investigation, this system has been deployed outdoors for multilateration measurements with distances up to 73 m in order to determine the reference point of a VLBI radio telescope at the Geodetic Observatory Wettzell.

An uncertainty budget was first established for the distances measured by the multilateration system. The uncertainties were around 21 µm with a maximum value of 44 µm for a distance of 73 m. However, it was shown that the position of head B1 drifted over time due to a mechanical instability of the tripod on which it was installed. The strategy to solve this was to define a new position of this head at each new day.

Then, a multilateration algorithm with self-calibration was applied on the measured distances, and thus the positions of the measurement heads and targets were determined, as well as their uncertainty. The difference between the distances measured by the telemetric system and those deduced from the coordinates provided by the multilateration algorithm yields a standard deviation of 27 µm. This standard deviation is slightly larger than expected because of the mechanical instability of the head B1: if we only study the results concerning this head, a standard deviation of 44 µm is obtained. The standard deviations for the other heads are compatible with the uncertainties previously determined.

The analysis of the uncertainties of the three-dimensional positions revealed a weakness in the configuration of the measurement head positions, with a larger uncertainty along the z axis as a consequence. Despite this, the magnitudes of the uncertainties for the targets set up on the radio telescope were compatible with our objective, i.e. defining the reference point of the telescope to better than 1 mm. In contrast, the positions of the survey pillars had large uncertainties, between 0.27 mm and 2.32 mm due to the unfavourable geometrical configuration. These positions are crucial for the knowledge of the VLBI reference point in the frame of the local site network at GOW, and, thus, of the local tie vectors describing the distances and orientations between the reference points of the hosted space geodetic techniques.

The use of a prototype instrument for the determination of the VLBI reference point involves risks. Thus, during this measurement campaign, two commercial total stations, which are well-proven instruments, have also been used to complete the multilateration measurements. At the end, a global network adjustment was performed combining the three instruments, and the reference point of the radio telescope was extracted. The estimated coordinates of the reference point show standard

deviations between 0.04 mm and 0.10 mm. Thus, the global objective aimed by GGOS was achieved with coordinates at least one order of magnitude more accurate than expected.

In addition, we have demonstrated that the developed prototype of multilateration system can be used outdoors, over distances up to 73 m, and with a significant lower uncertainty than commercial total stations. Nevertheless, the obtained results could have been better with a mechanically more stable head B1 and a more optimal head arrangement.

Declaration of competing interest

The authors declare the following financial interests/personal relationships which may be considered as potential competing interests: Joffray Guillory reports financial support was provided by EURAMET European Metrology Programme for Innovation and Research.

Acknowledgement

This work was partially funded by the Joint Research Project (JRP) 18SIB01 GeoMetre, project that received funding from the European Metrology Programme for Innovation and Research (EMPIR) co-financed by the participating states and from the European Union's Horizon 2020 research and innovation programme.

References

[1] Rothacher M, Beutler G, Behrend D, Donnellan A, Hinderer J, Ma C, Noll C, Oberst J, Pearlman M, Plag H-P, Richter B, Schöne T, Tavernier G, Woodworth PL. In: Plag H-P, Pearlman M, editors. Global geodetic observing system - meeting the requirements of a global society on a changing planet. Springer; 2020". p. 237–72. https://doi.org/10.1007/978-3-642-02687-4. 2009.

[2] Leinen S, Becker M, Dow J, Feltens J, Sauermann K. Geodetic determination of radio telescope antenna reference point and rotation axis parameters. J Survey Eng 2007;133(2):71. https://doi.org/10.1061/(ASCE)0733-9453(2007)133:2(41). 51.

[3] Li J, Xiong F, Yu C, Zhang J, Guo L, Fan Q. Precise determination of the reference point coordinates of Shanghai Tianma 65-m radio telescope. Chin Sci Bull 2014;59 (21):1861–9541. https://doi.org/10.1007/s11434-014-0349-8.

[4] Lanotte R, Pirri M, Bianco G. Matera site survey and VLBI invariant point determination". St. Petersburg, Russia: Proceedings of The 5th IVS General Meeting; 2008.

[5] Ning T, Haas R, Elgered G. Determination of the local tie vector between the VLBI and GNSS reference points at Onsala using GPS measurements. J Geodes 2015;89 (7):711–23. https://doi.org/10.1007/s00190-015-0809-1.

[6] Kallio U, Poutanen M. "Can we really promise a mm-accuracy for the local ties on a geo-VLBI antenna", Geodesy for Planet Earth. In: Kenyon S, Pacino M, Marti U, editors. Proceedings of the 2009 IAG symposium, buenos aires, Argentina. International association of geodesy symposia, vol. 136. Springer; 2009. p. 35–42. https://doi.org/10.1007/978-3-642-20338-1_5. 2012.

[7] Guillory J, Truong D, Wallerand J-P. Assessment of the mechanical errors of a prototype of an optical multilateration system. Rev Sci Instrum 2020;91(issue 2): 025004. https://doi.org/10.1063/1.5132933.

[8] Guillory J, Truong D, Wallerand J-P. Uncertainty assessment of a prototype of multilateration coordinate measurement system. Precis Eng 2020;66:496–506. https://doi.org/10.1016/j.precisioneng.2020.08.002.

[9] Guillory J, Truong D, Wallerand J-P. Multilateration with self-calibration: uncertainty assessment, experimental measurements and Monte-Carlo simulations. Metro 2022;2(issue 2):241–62. https://doi.org/10.3390/metrology2020015.

[10] Zha J, Wang T, Li L, Chen Y. Volumetric error compensation of machine tool using laser tracer and machining verification. Int J Adv Des Manuf Technol 2020;108(7): 2467–81. https://doi.org/10.1007/s00170-020-05556-8.

[11] Brecher C, Behrens J, Flore J, Wenzel C. Comprehensive calibration of robots and large machine tools using high precision laser-multilateration", Laser Metrology and Machine Performance X. 2013. p. 161–70.

[12] Nitsche J, Franke M, Haverkamp N, Heißelmann D. Six-degree-of-freedom pose estimation with µm/µrad accuracy based on laser multilateration. J Sens Sens Syst 2021;10(1):19–24. https://doi.org/10.5194/jsss-10-19-2021.

[13] Rafeld EK, Koppert N, Franke M, Keller F, Heißelmann D, Stein M, Kniel K. Recent developments on an interferometric multilateration measurement system for large volume coordinate metrology. Meas Sci Technol 2022;33(3):035004. https://doi.org/10.1088/1361-6501/ac407c.

[14] Nguyen QK, Kim S, Han SH, Ro SK, Kim SW, Kim YJ, Kim W, Oh JS. Improved self-calibration of a multilateration system based on absolute distance measurement. Sensors 2020;20(24):7288. https://doi.org/10.3390/s20247288.

[15] Hughes B, Campbell MA, Lewis AJ, Lazzarini GM, Kay N. Development of a high-accuracy multi-sensor, multi-target coordinate metrology system using frequency scanning interferometry and multilateration. In: Proceedings of society of photo-optical instrumentation engineers (SPIE); 2017, 1033202. https://doi.org/10.1117/12.2273644. 10332, Videometrics, Range Imaging, and Applications XIV.

[16] Kamugasa SW, Rothacher M, Gayde J-C, Mainaud Durand H. Development and validation of a multilateration test bench for particle accelerator pre-alignment. Meas Sci Technol 2018;29(3):034010. https://doi.org/10.1088/1361-6501/aa9f84.

[17] Dawson J, Sarti P, Johnston GM, Vittuari L. Indirect approach to invariant point determination for SLR and VLBI systems: an assessment. J Geodes 2007;81(6): 433–41. https://doi.org/10.1007/s00190-006-0125-x.

[18] Lin Y, Zhang G. The optimal arrangement of four laser tracking interferometers in 3D coordinate measuring system based on multi-lateration. In: Proceedings of the international symposium on virtual environments, human-computer interfaces and measurement systems (VECIMS); July 2003. https://doi.org/10.1109/VECIMS.2003.1227044. Lugano, Switzerland.

[19] Edlén B. The refractive index of air. Metrologia 1966;2(2):71–80. https://doi.org/10.1088/0026-1394/2/2/002.

[20] Ciddor PE. Refractive index of air: new equations for the visible and near infrared. Appl Opt 1996;35(9):1566. https://doi.org/10.1364/AO.35.001566.

[21] Guillory J, Truong D, Wallerand J-P, Alexandre C. Absolute multilateration-based coordinate measurement system using retroreflecting glass spheres. Precis Eng 2022;73:214–27. https://doi.org/10.1016/j.precisioneng.2021.09.009.

[22] Mitchell J, Spence A, Hoang M, Free A. Sensor fusion of laser trackers for use in large-scale precision metrology. In: Proceedings of photonics technologies for robotics, automation, and manufacturing; 2003. https://doi.org/10.1117/12.515021. Providence, Rhode Island.

[23] Lösler M, Eschelbach C, Mähler S, Guillory J, Truong D, Wallerand J-P. Operator-software impact in local tie networks: case study at geodetic observatory Wettzell. Appl Geomat 2023;15(1):77–95. https://doi.org/10.1007/s12518-022-00477-5.

[24] Crocetto N, Gatti M, Russo P. Simplified formulae for the BIQUE estimation of variance components in disjunctive observation groups. J Geodes 2000;74(6): 447–57. https://doi.org/10.1007/s001900000109.

[25] Lösler M, Eschelbach C, Riepl S. A modified approach for automated reference point determination of SLR and VLBI telescopes. Technisches Messen 2018;85(10): 616–26. https://doi.org/10.1515/teme-2018-0053.

[26] Lösler M, Eschelbach C, Klügel T, Riepl S. ILRS reference point determination using close range photogrammetry. Appl Sci 2021;11(6):2785. https://doi.org/10.3390/app11062785.